Nonlinear PWM-Controlled Single-Phase Boost Mode Grid-Connected Photovoltaic Inverter With Limited Storage Inductance Current

Daolian Chen, *Senior Member, IEEE*, Yanhui Qiu, Yiwen Chen, and Yongji He

***Abstract*—A nonlinear pulse width modulation-controlled single-phase boost mode photovoltaic grid-connected inverter with limited storage inductance current is proposed in this paper. The circuit topology, control strategy, steady-state principle characteristic, and design criterion for the key circuit parameters of this kind of inverter are investigated in depth, and important conclusions are obtained. The inverter's regenerating energy duty ratio 1–*D* which decreases with the decline of the grid-connected voltage is real time adapted by sampling and feeding back the inverting bridge modulation current, and the average value of the modulation current in each switching cycle tracks the reference sinusoidal signal to get high-quality grid-connected current. The active control of the energy storage inductance current and the balance of the voltage step-up ratio are realized by adding a bypass switch connected in parallel with the energy storage inductance and using two kinds of switching pattern namely boost pattern and freewheeling pattern. The theoretical analysis and experimental results of the 1 kVA 110 VDC/220 V50 Hz photovoltaic grid-connected inverter prototype show that it has the advantages such as single-stage boost conversion, high conversion efficiency, high quality of grid-connected current waveform, low value of energy storage inductance, simple control, etc.**

***Index Terms*—Boost mode, limited storage inductance current, nonlinear pulse width modulation (PWM) control, photovoltaic (PV) grid-connected inverter, single-phase.**

I. Introduction

THE single stage inverter has become a research hotspot in the new energy power-generating field [1]–[8]. Compared with the buck mode inverter, the boost mode inverter has the advantages of single-stage voltage boosting, direct control of the output current and easy realizing the maximum power point tracking (MPPT) of the photovoltaic (PV) cell, long life of the energy storage inductors' components, timely protection with over current and high system reliability, etc. In recent years, with the emergence of new type devices such as bidirectional blocking insulated-gate bipolar transistor (IGBT) and the development of superconducting technology, boost mode inverter will have a more important application value.

Three-phase boost mode grid-connected inverter adopting a two-loop control strategy with motor speed outer loop and dc link current inner loop has obtained better performance [5]. The one-cycle control method derived by the buck dc–dc converter has also been applied for three-phase boost-type grid-connected inverter [6]. However, the traditional single-phase boost mode sinusoidal pulse width modulation (PWM) inverter does not meet the basic principle of boost converter when the output voltage is lower than the input voltage. Namely whether the energy storage inductance L is magnetizing or regenerating energy, its current is always increasing, which lead to inverter cannot get sinusoidal grid-connected current. Therefore, the inverter whose regenerating duty ratio 1–D is increasing with the decreasing of the grid-connected voltage u_{n} has inherent defects such as large energy storage inductor and its current, serious output waveform distortion, and low conversion efficiency. For all this, some new solutions on circuit topology and control strategy are proposed [7]–[15].

A current-fed Z-source inverter has been proposed which can successfully buck and boost voltage in [7], but this inverter has more complex circuit topology due to overmuch energy storage element amount. A one-cycle controlled single-phase Z-source inverter with unsymmetrical characteristic is proposed in [8]. This inverter has simple circuit topology, input and output sharing the same ground, but it can only buck voltage; the conversion efficiency and total harmonic distortion (THD) of the output voltage are not given. A differential inverter in which two bidirectional boost dc–dc converters are connected in parallel in the input side and connected in series reversely in the output side is proposed in [9] and [10]. The two bidirectional boost dc–dc converters operate simultaneously and, respectively, output low-frequency pulsating sinusoidal voltage with the same dc component and 180° phase difference. And sinusoidal voltage is obtained on the output load. But it is hard to get ideal conversion efficiency of the inverter because of the loop current from the simultaneous operating of the two converters. An inverter whose power switch is connected in series between the positive end of the input source and energy storage inductor, and a freewheeling diode is connected in parallel between the negative end of the input source and energy storage inductor in the traditional circuit is proposed in [11]. The serial-connected power switch and the inverting bridge power switches are controlled

Manuscript received December 7, 2015; revised April 7, 2016; accepted March 8, 2016. Date of publication May 23, 2016; date of current version January 20, 2017. This work was supported by the Key Project of Natural Science Foundation of China under Grant 51537001. Recommended for publication by Associate Editor M. Vitelli.

The authors are with the Fujian Key Laboratory of New Energy Generation and Power Conversion, Fuzhou University, Fuzhou 350116, China (e-mail: chendaolian@hotmail.com; qyh522@sina.com; fzucyw@163.com; fzuhyj@sina.com).

Color versions of one or more of the figures in this paper are available online at http://ieeexplore.ieee.org.

Digital Object Identifier 10.1109/TPEL.2016.2571725

by the hysteresis control strategy of the output voltage and energy storage inductor current, the inverter is operating in boost mode or buck mode, and the dual sinusoidal half-wave energy storage inductor current and output sinusoidal voltage with high frequency (HF) ripple which are synchronized with the output voltage are obtained. This scheme reduces the energy storage inductor to 0.3 mH, but the output filter capacitance is still as high as 20 μF; the conversion efficiency is only 78% and THD of the output voltage is as high as 3.87%. A single-phase boost mode inverter with HF link whose output and input end connects in parallel with a flyback ac–dc energy regenerating circuit is proposed in [12]. The flyback ac–dc energy regenerating circuit operates only when the output voltage is falling and the absolute value of the output voltage is smaller or equal to the input voltage multiplied by turn ratio of the transformer. The experimental waveforms are not given and this scheme is at the cost of increasing the complexity of the circuit. An active nonlinear modulation control strategy is proposed in [13]. Based on the derived nonlinear modulation compensation function restraining harmonic waves of the grid-connected current, the proposed control strategy, respectively, extracts the dc and ac components of the energy storage inductance current and compares with the grid-connected current reference to get the nonlinear PWM signal which can inhibit third harmonic wave of the grid-connected current. The proposed control strategy can effectively suppress the third harmonic wave of the grid-connected current, but there still are defects such as large energy storage inductance (21 mH) and THD of the output current waveform up to 4.42%. A control strategy based on the inverter's output current involving feedforward and feedback terms is proposed in [14], which improves the quality of output waveforms, but the energy storage inductance *L* is still as high as 10 mH; the conversion efficiency and THD of the output voltage are not given. A parallel resonator is connected in series between the input source and energy storage inductor of the traditional inverter, and an output voltage and current feedback control strategy with proportional resonant is adopted in [15]. The parallel resonator can filter out the second and fourth low-frequency harmonic component in energy storage inductor current and reduce the energy storage inductor and the input low-frequency ripple to some extent. The control strategy effectively improves the quality of output waveform, but the resonant inductors in the parallel resonator are high up to 5 and 10 mH and the energy storage inductor value of the inverter is 5 mH. Only light-load waveform is provided and the conversion efficiency is not provided.

To overcome inherent defects of the traditional single-phase boost mode inverter, a nonlinear PWM-controlled single-phase boost mode PV grid-connected inverter with limited energy storage inductance current is proposed and deeply researched in this paper, and important conclusions are obtained.

II. Nonlinear PWM Control Strategy

A. Control Principle

In order to improve the quality of output waveform of the traditional single-phase boost mode inverter, a new idea that regenerating duty ratio 1–*D* of the inverter decreases with the decline of the grid-connected voltage u_n, namely a nonlinear

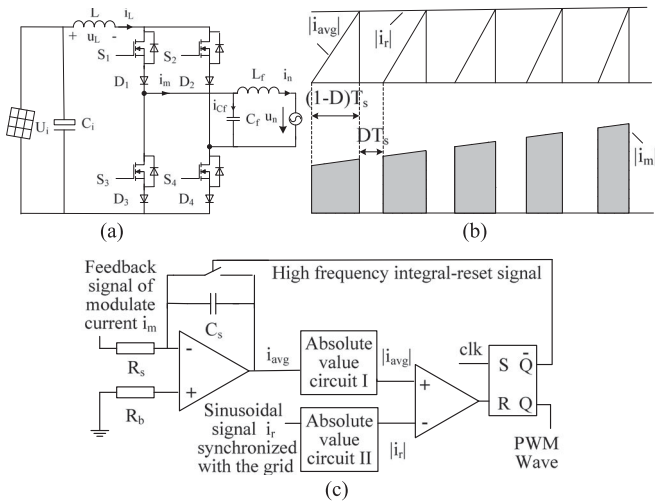

Fig. 1. Circuit topology of traditional single-phase boost mode inverter and nonlinear PWM control strategy. (a) Circuit topology. (b) Control principle waveform. (c) Control circuit block.

PWM control strategy based on inverting bridge's modulation current is proposed in this paper, as shown in Fig. 1. This control strategy is that the inverter's regenerating energy duty ratio 1–*D* is real time regulated by detecting and feeding back the modulation current i_{m} and high-quality grid-connected current is obtained. When the grid voltage u_n is less than the input voltage U_i, i_m is greater than the expected value and the integral time (1–*D*) T_s of the feedback signal i_m to the reference value $|i_r|$ will become shorter, 1–*D* will be decreased; thus, the waveform quality of the grid-connected current i_n will be improved.

Set the switching period is T_s, and the integral circuit's time constant is $R_sC_s = T_s$. After the modulation current feedback signal i_m of the inverter through the integral circuit and the absolute value circuit, the average value i_{avg} of i_m is obtained, and its absolute value $|i_{\mathrm{avg}}|$ can be derived as follows:

$$|i_{avg}| = \frac{1}{R_sC_s}\left|\int_0^{(1-D)T_s} i_m \mathrm{d}t\right| = \frac{1}{T_s}\left|\int_0^{(1-D)T_s} i_m \mathrm{d}t\right|. \tag{1}$$

The average value of harmonic current in C_{f} within one T_s is zero; thus, the average value of output filtering capacitance current i_{Cf} within one T_s is the average value of its fundamental wave component i_{Cf1}, namely

$$\frac{1}{T_s}\int_0^{(1-D)T_s} i_m \mathrm{d}t = \frac{1}{T_s}\int_0^{T_s} i_{Cf1}\mathrm{d}t + \frac{1}{T_s}\int_0^{T_s} i_n \mathrm{d}t \overset{\text{most range of load}}{\approx} \frac{1}{T_s}\int_0^{T_s} i_n \mathrm{d}t. \tag{2}$$

Equations (1) and (2) show that the average value of i_n approximately equals to i_{avg} within one T_s. Therefore, i_n can be controlled by controlling the reference signal i_r. When U_i changes, the constant of i_n is realized by adjusting 1–*D*. As i_m is nearly constant during (1–*D*) T_s, derived from (1)

$$|i_m(1-D)| = |i_{\mathrm{avg}}| = |i_r|. \tag{3}$$

Derived from (3)

$$1 - D = |i_r / i_m| . \tag{4}$$

Equation (4) shows that 1–*D* is proportional to $|i_r/i_m|$ and is not proportional to the error current $i_r - i_m$. Therefore, the control strategy is called nonlinear PWM control strategy.

B. New Problems Caused by the Proposed Control Strategy

Nonlinear PWM control strategy directly determines 1–*D* and improves the output waveform. However, the larger the u_n and i_n of the inverter, the smaller the *D*; the greater the 1–*D* and the smaller the step-up ratio $1/(1-D)$, which does not meet the control requirements of the boost converter, namely the variation law of *D* is opposite to that of *D* required by the step-up ratio of the inverter. When u_n and i_n are the maximum, *D* is the minimum $D_{\min}$, the magnetizing time of the energy storage inductor is the shortest, the demagnetizing time is the longest, and demagnetizing voltage is the largest; i_L is most easily discontinuous. In order to ensure proper operation, i_L must be designed on critical continuous state at least when u_n , i_n are the largest and $D = D_{\min}$, namely $1/(1-D_{\min}) \geq u_n/U_i$. Thus, a new problem is caused: when $D > D_{\min}$, the step-up ratio is too large and the energy of the energy storage inductors is excess.

In order to satisfy the control requirements of the boost converter, this kind of nonlinear PWM-controlled inverter needs to balance the excess energy of the energy storage inductor and too large step-up ratio by the loss of internal resistance including energy storage inductor's parasitic resistance and power switches conduction resistance, which leads to inherent defects such as large internal resistance loss and low conversion efficiency.

III. Solutions to Excess Inductor Energy and too Larger Step-up Ratio

A. Two Kinds of Switching Pattern

In order to solve problems such as the excess energy of the energy storage inductor, too large step-up ratio, large internal resistance loss and low conversion efficiency for $D > D_{\min}$, it needs to limit the energy storage inductor current i_L. It is necessary to add a free-wheeling pattern of the energy storage inductor to limit $i_{\rm L}$ and transfer its excess energy to the ac grid in the subsequent several switching periods, as shown in Fig. 2. In Fig. 2, ${I_L}^*$ is the limitation value for i_L, $T_{\rm es}$ is the equivalent switching period, and $D_{\rm I1}, D_{{\rm II}i} (i = 1, 2)$ are the duty ratio of the inverter in the boost pattern and the free-wheeling pattern, respectively.

In order to limit the energy storage inductor current, a two-quadrant bypass switch is connected in parallel at both ends of the inductance *L*, which is consisting of S_0 and D_0 connected in series, as shown in Fig. 3(a).

The additional bypass switch can actively control i_L. Once i_L is greater than the limitation value ${I_L}^*$, the energy storage inductor freewheeling state when S_0 is conducted replaces the energy storage inductor magnetizing state when the inverting bridge switches are shoot-through, which can effectively

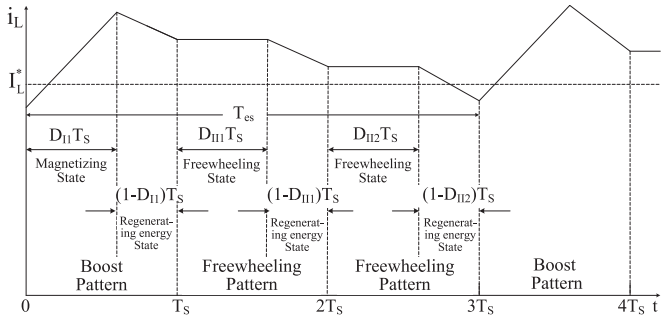

Fig. 2. Waveform of energy storage inductor current with free-wheeling pattern.

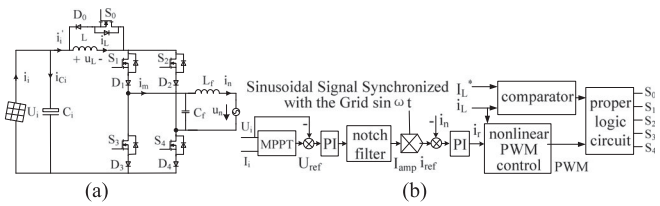

Fig. 3. Circuit topology and control strategy of the proposed inverter. (a) Circuit topology. (b) Control block diagram.

suppress the rise of the energy storage inductor current, and solve the problems of too large step-up ratio of the inverter and excess energy of the energy storage inductance.

The two types of switching pattern which can limit the energy storage inductor current: When $i_L < I_L^*$, the magnetizing state of the energy storage inductors through the pass-through bridge arm during the DT_s and the regenerating energy state of the energy storage inductors to the grid during (1–*D*) T_s are called the switching pattern I-boost pattern; when $i_L > I_L^*$, the freewheeling state of the energy storage inductor through the bypass switch S_0 during the DT_s and the regenerating energy state of the energy storage inductors to the grid during (1–D) T_s are called the switching pattern II-freewheeling pattern. Three-loop control strategy which consists of the inner loop of the nonlinear PWM control based on the modulation current, the central loop of the grid-connected current, and the outer power loop of the MPPT shown in Fig. 3(b) is introduced in the proposed inverter with two kinds of switching pattern and limitation of the energy storage inductor current. It is necessary to add that i_m is i_L during (1–*D*) T_s, namely i_m of the nonlinear PWM control loop shown in Fig. 1(c) can be replaced by the energy storage inductor current i_L shown in Fig. 3(b); the MPPT is a dual-mode MPPT which is combination of open-circuit voltage and disturbance observation.

B. Energy Storage Inductor Current Limitation Value

Set the grid power factor equals 1, the grid voltage and grid-connected current are, respectively

$$u_n(t) = \sqrt{2} U_n \sin(\omega t) \tag{5}$$

$$i_n(t) = \sqrt{2} I_n \sin(\omega t). \tag{6}$$

The average value of i_n and i_m during kth T_s is equal, as in

$$\frac{1}{T_s}\int_{(k-1)T_s}^{kT_s}\sqrt{2}I_n\sin(\omega t)dt = \frac{1}{T_s}\int_{(k-1+D)T_s}^{kT_s}\left\{\int_{(k-1+D)T_s}^{t}\frac{U_i-\left|\sqrt{2}U_n\sin(\omega\tau)\right|}{L}d\tau + i_L(k-1+D)T_s\right\}\mathrm{dt}. \quad (7)$$

When $|u_n| > U_i$, the freewheeling pattern adjusts the relationship between 1–*D* and the step-up ratio. The number of the freewheeling pattern reduces with the rise of $|u_n|$. At the same time, *L* needs enough magnetizing time to guarantee i_L continuous, i.e., operating in switching pattern I. So, the regenerating energy duty ratio of the inverter cannot be too large, as follows:

$$1/(1-D) \geq |u_n(kT_s)|/U_i. \quad (8)$$

The extreme situation of (8) is that i_n and u_n reach the peak simultaneously. At the moment, 1–*D* of corresponding switching period is the maximum, *L* has longest demagnetizing time and highest demagnetizing rate, and i_L rapidly decreases to the minimum value leading it discontinuous. When $\omega t = \pi/2$, set $k = (\pi/2)/(\omega T_s)$, substituting them into (7)

$$i_L(k-1+D)T_s = \frac{\sqrt{2}I_n}{1-D} - \frac{(U_i-\sqrt{2}U_n)(1-D)}{2Lf_s}. \quad (9)$$

Derived from (8) and (9)

$$i_L[(k-1+D)T_s] \geq 2\frac{U_nI_n}{U_i} + U_i\frac{\sqrt{2}U_n-U_i}{\sqrt{2}U_nLf_s}. \quad (10)$$

So, the limitation value of the energy storage inductor current must be satisfied

$$I_L^* \geq 2\frac{P_n}{U_i} + U_i\frac{\sqrt{2}U_n-U_i}{\sqrt{2}U_nLf_s}. \quad (11)$$

In order to reduce loss, i_L should be as small as possible. The minimum limitation value ${I_L}^*$ can be directly derived from (11). At this time, the maximum regenerating energy duty ratio should be satisfied by (8), namely $1-D_{\min} = U_i/\sqrt{2}U_n$. In addition, the bigger the *L* and f_s, the more stable the i_L. When Lf_s is big enough, $2P_n/U_i \gg U_i(\sqrt{2}U_n-U_i)/(\sqrt{2}U_nLf_s)$, derived as follows:

$$i_L = I_L^* \approx 2P_n/U_i. \quad (12)$$

The regenerating energy duty ratio can be derived from (4), (6), and (12)

$$1-D \approx \sqrt{2}\frac{I_n}{i_L}|\sin(\omega t)| = \frac{U_i}{\sqrt{2}U_n}|\sin(\omega t)|. \quad (13)$$

From (11), ${I_L}^*$ mainly depends on the output power of PV cells for the inverter. If the illumination, the temperature, and the peak value of the grid voltage are constant, I_L* will remain unchanged.

IV. Steady Principle Characteristics

A. Equivalent Circuit and Operating Modes in Low Frequency (LF) Output Period

According to the relative value u_n/U_i, the inverter's switching pattern I or II, and the polarity of the modulation current i_m, the proposed inverter has six kinds of equivalent circuits and A, B, C, D, E, F six operating modes within a LF output period (t_0–t_8), as shown in Fig. 4 and Table I.

B. Operating Principle of Intervals

There are eight operating intervals for the inverter within an LF output period (t_0–t_8), as shown in Fig. 4(g).

[t_0–t_1]: $0 < u_n < U_i$, operating in Mode A. *L* is freewheeling during DT_s and magnetizing during (1–*D*) T_s. i_L keeps rising, $i_L > {I_L}^*$. The inverter operates in switching pattern II corresponding to the equivalent circuit, as shown in Fig. 4(e) and (c). Since 1–*D* is quiet small around u_n's zero point, i_L rises slowly. u_n rises to the U_i and i_L reaches its maximum value $i_{L\max}$ at the time t_1. Considering (13), derived as

$$\begin{aligned} i_{L\max} &= \sum_{k=-\alpha f_s/\omega}^{\alpha f_s/\omega}\frac{U_i-\sqrt{2}U_n\left|\sin(\omega kT_s)\right|}{L}[1-D(k)]T_s + I_L^* \\ &= \int_{-\alpha f_s/\omega}^{\alpha f_s/\omega}\frac{U_i-\sqrt{2}U_n\left|\sin(\omega t)\right|}{L}\frac{U_i}{\sqrt{2}U_n}\left|\sin(\omega t)\right|dt + I_L^* \\ &= \frac{U_i}{\sqrt{2}U_n\omega L}\left[2U_i(1-\cos\alpha) + \frac{U_n(\sin 2\alpha - 2\alpha)}{\sqrt{2}}\right] + I_L^*. \end{aligned} \quad (14)$$

The angle α is the corresponding angle when $u_n = U_i$, namely

$$\alpha = \omega(t_1-t_0) = \arcsin\frac{U_i}{\sqrt{2}U_n}. \quad (15)$$

[t_1–t_2]: $u_n > U_i$, operating in Mode B. L is freewheeling during DT_s and demagnetizing during (1–*D*) T_s. $i_L > {I_L}^*$, the inverter operates in switching pattern II corresponding to the equivalent circuit, as shown in Fig. 4(e) and (c). After every T_s period, i_L is always higher than ${I_L}^*$ and decreasing, 1–*D* is increasing, and the drop rate of i_L is increasing. At moment t_2, i_L rapidly drops back within ${I_L}^*$. The angle β is the corresponding angle of i_L from the maximum value at t_1 to within ${I_L}^*$ at t_2, namely $\beta = \omega(t_2-t_1)$. Set $i_L(t_2) = {I_L}^*$, since the decline value of i_L from t_1 to t_2 is equal to the difference between $i_{L\max}$ and ${I_L}^*$, derived as

$$\begin{aligned} &\sum_{k=-\alpha f_s/\omega}^{\alpha f_s/\omega}\frac{U_i-\sqrt{2}U_n\left|\sin(\omega kT_s)\right|}{L}\frac{U_i}{\sqrt{2}U_n}\left|\sin(\omega kT_s)\right|T_s \\ &= \sum_{k=\alpha f_s/\omega}^{(\alpha+\beta)f_s/\omega}\frac{\sqrt{2}U_n\sin(\omega kT_s)-U_i}{L}\frac{U_i}{\sqrt{2}U_n}\sin(\omega kT_s)T_s. \end{aligned} \quad (16)$$

Derived from (16), β is satisfied as

$$\sin\alpha\cos(\alpha+\beta) + \sin 2(\alpha+\beta)/4 + \beta/2 = 2\sin\alpha - \sin(2\alpha)/(4-\alpha). \quad (17)$$

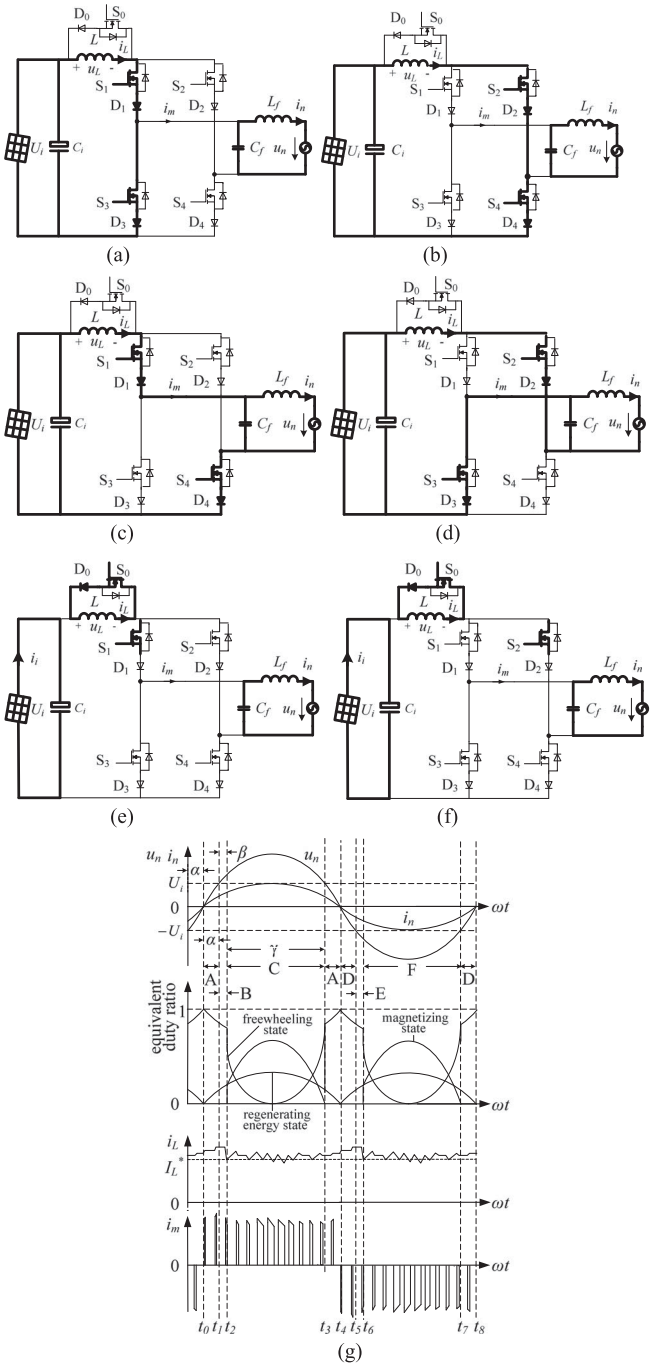

Fig. 4. Equivalent circuit and steady principle waveform of the inverter. (a) Magnetizing state for $i_m > 0$. (b) Magnetizing state for $i_m < 0$. (c) Regenerating energy state for $i_m > 0$. (d) Regenerating energy state for $i_m < 0$. (e) Freewheeling state for $i_m > 0$. (f) Freewheeling state for $i_m < 0$. (g) Steady principle waveform within a LF output period.

$[t_2$–$t_3]$: $u_n > U_i$, operating in Mode C. i_L is in HF pulsing state around $I_L{}^*$, and switching patterns I and II operate alternately. If $i_L < I_L{}^*$ and the inverter operates in switching pattern I, L is magnetizing during DT_s and demagnetizing during (1–D) T_s, i_L is increasing, if $i_L > I_L^*$, the inverter operates in switching pattern II, L is freewheeling during DT_s and demagnetizing during (1–D) T_s, i_L is decreasing. Set from the kth T_s, the inverter continuously operates in switching mode I for m of T_s, and from(k+m)th T_s, the inverter continuously operates in switching mode II for n of T_s, ... in one $T_{\rm es}$, m and n are natural number, then i_L is back within $I_L{}^*$ again, the current variation of L can be approximately considered as zero, namely

$$\sum_{j=k}^{k+m-1} \frac{U_i}{L} D(j) T_s + \sum_{j=k}^{k+m+n-1} \frac{U_i - |u_n|}{L} [1 - D(j)] T_s = 0. \tag{18}$$

Combination (13) with (18), the equivalent duty ratios of magnetizing and freewheeling states during each $T_{\rm es}$, respectively, are

$$\sum_{j=k}^{k+m-1} \frac{D(j)}{m+n} = \sin^2(\omega t) - \frac{U_i}{\sqrt{2} U_n} \sin(\omega t) \tag{19}$$

$$\sum_{j=k+m}^{k+m+n-1} \frac{D(j)}{m+n} = \cos^2(\omega t). \tag{20}$$

The equivalent duty ratio of regenerating energy state during each $T_{\rm es}$ meets (13). The corresponding equivalent circuits of the three kinds of state for this interval are shown in Fig. 4(a), (e), and (c). The angle γ is the corresponding angle from i_L first dropping to $I_L{}^*$ at t_2 to u_n decreasing to U_i at t_3, namely

$$\gamma = \pi - 2\alpha - \beta. \tag{21}$$

$[t_3$–$t_4]$: $0 < u_n < U_i$, operating in Mode A. The operating principle is the same with that of the interval $[t_0$–$t_1]$. The angle α is the corresponding angle when u_n is decreasing from U_i to 0.

$[t_4$–$t_5]$: $0 > u_n > -U_i$, operating in Mode D. The corresponding equivalent circuits are shown in Fig. 4(f) and (d). The operating principle is the same with that of the interval $[t_0$–$t_1]$.

$[t_5$–$t_6]$: $u_n < -U_i$, operating in Mode E. The corresponding equivalent circuits are the same with those of Mode D. The operating principle is the same with that of the interval $[t_1$–$t_2]$.

$[t_6$–$t_7]$: $u_n < -U_i$, operating in Mode F. The corresponding equivalent circuits are shown in Fig. 4(b), (f), and (d). The operating principle is the same with that of the interval $[t_2$–$t_3]$.

$[t_7$–$t_8]$: $0 > u_n > -U_i$, operating in Mode D. The operating principle is the same with that of the interval $[t_4$–$t_5]$.

It can be seen that the LF operating modes' sequence of the inverter is A–B–C–A–D–E–F–D.

TABLE I
SIX OPERATING MODES IN ONE LF PERIOD

Operating mode	Corresponding interval	Comparing u_n with U_i	Changing law of i_L	Switching pattern
A	t_0–t_1, t_3–t_4	$0 < u_n < U_i$	$i_L > I_L*$ and increasing	II
B	t_1–t_2	$u_n > U_i$	$i_L > I_L*$ and decreasing	II
C	t_2–t_3	$u_n > U_i$	HF pulsing around I_L*	Alternating of I, II
D	t_4–t_5, t_7–t_8	$0 > u_n > -U_i$	$i_L > I_L*$ and increasing	II
E	t_5–t_6	$u_n < -U_i$	$i_L > I_L*$ and decreasing	II
F	t_6–t_7	$u_n < -U_i$	HF pulsingaround I_L*	Alternating of I, II

In addition, the current i_{S0} through S_0 under the freewheeling state is the energy storage inductor current i_L. If the HF switch current component is ignored and approximately consider $i_L = {I_L}^*$, i_{S0} is derived from (12) and (20) at the normal voltage boosting interval corresponding to operating Modes C and F

$$i_{S0} = 2P_n \cos^2(\omega t)/U_i = P_n[1-\cos(2\omega t)]/U_i. \quad (22)$$

The previous equation shows that the double line frequency component of the input-side current of the inverting bridge mainly flows through S_0; thus, the energy storage inductor of the inverter can be greatly reduced.

C. Equivalent Step-up Ratio

When L and ${I_L}^*$ are large enough and the inverter is operating in two kinds of switching pattern, i_L is basically stable and approximately considered as $i_L \approx I_L^*$. According to the control idea of limitation of the energy storage inductor current, the equivalent switching period $T_{\rm es}$ can be used to further describe the inverter's operating principle in operating Modes C and F. $T_{\rm es} = (m+n)T_s$ and the equivalent duty ratios of magnetizing, freewheeling and regenerating energy states during each $T_{\rm es}$ are also, respectively, expressed as $D_{e1} = \frac{T_s}{T_{es}} \sum_{i=1}^{m} D_{Ii}$, $D_{e2} = \frac{T_s}{T_{es}} \sum_{i=1}^{m} D_{IIi}$, and $1–D_{e1} – D_{e2}$. Taking $m=1, n=2$ as an example, its principle is shown in Fig. 2. When $t=0$, $i_L < {I_L}^*$. $i_L > {I_L}^*$ after $m\,T_s$, i_L drops back within I_L* after $n\,T_s$.i_L approximately can be considered as constant after $(m+n)T_s$ namely one $T_{\rm es}$. *m*, *n* corresponding to each $T_{\rm es}$ are different in practice. Under the certain I_L^*, *m*/*n* increases with the increase of the amplitude of u_n, i_n.

By using the state-space average method, the steady-state values of switching state variables are derived as

$$i_L = \frac{u_i(1-D_{e2}) - u_n(1-D_{e1}-D_{e2})}{r_1(1-D_{e2}) + r_2(1-D_{e1}-D_{e2})^2 + r_3 D_{e2}} \quad (23a)$$

$$u_{Cf} = \frac{u_i r_2(1-D_{e2})(1-D_{e1}-D_{e2}) - u_n[r_1(1-D_{e2}) + r_3 D_{e2}]}{r_1(1-D_{e2}) + r_2(1-D_{e1}-D_{e2})^2 + r_3 D_{e2}} \quad (23b)$$

$$i_n = \frac{u_i(1-D_{e2})(1-D_{e1}-D_{e2}) - u_n(1-D_{e1}-D_{e2})^2}{r_1(1-D_{e2}) + r_2(1-D_{e1}-D_{e2})^2 + r_3 D_{e2}}. \quad (23c)$$

In (23), r_1 is the equivalent resistance including the input voltage source, energy storage inductor, power switches and blocking diode, r_2 is the equivalent resistance including ac power grid and the output filter inductance, and r_3 is the equivalent resistance of the bypass switch.

Because all power switches of the inverting bridge are connected in serial with the blocking diode, the energy storage inductor current i_L can only flow positively and the inverter can only operate in the first quadrant. If ignore the equivalent resistors r_1, r_2, and r_3, the relationship between step-up ratio and duty ratio of the equivalent switch in the ideal situation is

$$\frac{u_{Cf}}{u_i} = \frac{u_n}{u_i} = 1 + \frac{D_{e1}}{1-D_{e1}-D_{e2}}. \quad (24)$$

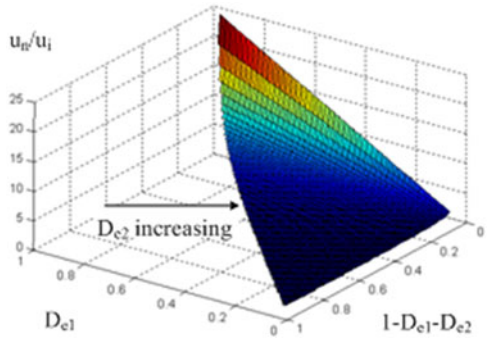

Fig. 5. Relationship between duty ratio of equivalent switch period and voltage step-up ratio.

The previous equation can be expressed as Fig. 5. Thus, under certain $1–D_{e1} – D_{e2}$, the more the number of freewheeling states, namely the greater the D_{e2}, the smaller the step-up ratio. So, D_{e2} can balance regenerating energy time and step-up ratio without affecting i_L.

D. Analysis of HF Switching Process

In order to guarantee i_L continuous, the commutation overlap time of the power switch should be set. According to the relative size of i_L and ${I_L}^*$, u_n and U_i and the relationship of the polarity of u_n, i_m, the HF switching process of the inverter is divided into four kinds of situation and only $i_m > 0$ corresponding to Fig. 4(a), (c), and (e) is given, as shown in Fig. 6. Taking Fig. 6(a) corresponding to Fig. 4(c) and (e) as an example, S_1 is conducted, S_2, S_3 are cut-off. Considering the influence of the junction capacitance of the power switches, the switching process t_0–t_8 is divided into eight intervals.

[t_0–t_1]: at t_0, S_0 is conducted, S_4 is turned off. Since the voltage stress of D_4 is $u_{D4} = (U_i - u_n)/2, S_4$ can be turned off with zero voltage and zero current. During the interval, the voltage stress of $D_3 u_{D3} = (U_i - u_n)/2, L$ is freewheeling, i_L remains the constant, $i_m = 0$, the output filter maintains the grid current.

[t_1–t_2]: at t_1, S_0 is still conducted, S_4 can be turned on with zero-voltage and zero-current since D_4 is under reverse blocking, $i_{s4} = 0$. The operating state of the inverter is similar to the interval t_0–t_1.

[t_2–t_3]: at t_2, S_4 is still conducted, S_0 is hard turned off. i_L is charging the junction capacitance $C_{\rm ds0}$ of S_0. The terminal voltage $u_{\rm ds0}$ of S_0 is rapidly rising, u_{D3} and $u_{\rm D4}$ are rapidly decreasing, u_L is increasing reversely, i_L starts dropping, $i_m = 0$, and the output filter maintains the grid current.

[t_3–t_4]: at t_3, S_4 is still conducted, the positive voltage stress of $S_0 u_{ds0} = u_n - U_i, u_{D3} = u_{D4} = 0, i_{s4}$ is rapidly rising and i_{s0} rapidly decreasing, $i_{s0} + i_{s4} = i_L$. S_0 and S_4 are in commuting current process; the inverter converts from DT_S to (1–*D*) T_S. During the interval, $u_L = U_i - u_n, i_L$ is decreasing, *L* is demagnetizing, i_m starts increasing from zero, U_i and *L* transfer energy to the output side.

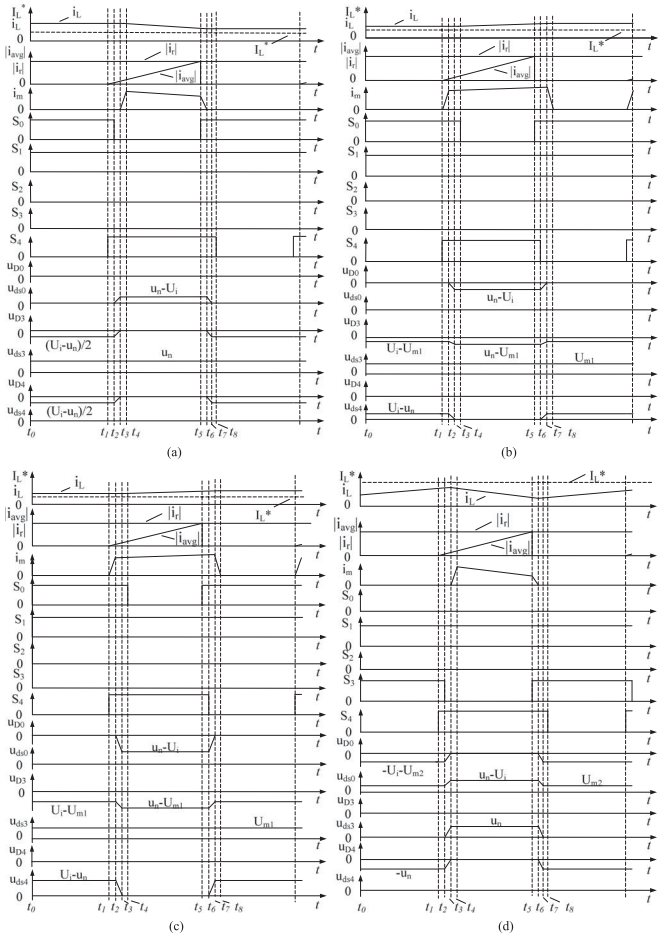

Fig. 6. HF switching process when $i_m > 0$. (a) $i_L > I_L{}^*$, $U_i < u_n$. (b) $i_L > I_L{}^*$, $U_i > u_n > 0$. (c) $i_L > I_L{}^*$, $0 > u_n$. (d) $i_L < I_L{}^*$, $U_i < u_n$.

[t_4–t_5]: at t_4, S_4 is still conducted, S_0 is completely turned off, and the commutation process is over. $i_m = i_L$ during the interval.

[t_5–t_6]: at t_5, S_4 is still conducted, S_0 is hard turned on. i_{s0} is rapidly rising, $u_{\mathrm{ds}0} = u_n - U_i$, i_{s4} is rapidly decreasing, $i_{s0} + i_{s4} = i_L$, S_0 and S_4 are in commutation process, the inverter converts from (1–*D*) T_s to DT_S. The modulating current i_m of the output side of the inverter bridge is rapidly decreasing.

[t_6–t_7]: at t_6, the commutation process is over, i_{s0} rises to $i_{s0} = i_L, i_{s4} = 0$, $C_{\mathrm{ds}0}$ starts discharging and makes $u_{\mathrm{ds}0}$ decreases rapidly from $u_n - U_i$, and D_3 and D_4 start to take reverse voltage stress and u_{D3} and u_{D4} are rapidly rising. During the interval $i_m = 0$, the output filter maintains the grid current.

[t_7–t_8]: at t_7, S_4 is still conducted, and S_0 is completely turned on. During the interval, $u_{D3} = u_{D4} = (U_i - u_n)/2, u_L = 0, L$ is freewheeling, i_L remains constant, $i_m = 0$, and the output filter maintains the grid current.

V. Designing Criterion for Key Circuit Parameters

A. Design for Energy Storage Inductor

Known from (11), for certain P_n, U_i, and u_n, the larger the Lf_s, the smaller the allowed $I_L{}^*$. Set $k_L\%$ to be the pulsating ratio, the pulsating ratio of i_L in one T_s is $\Delta i_L / i_L \le k_L\%$; considering (12), it can be derived

$$Lf_s \ge \frac{1}{2}\left[k_L\%^{-1} - \left(1 + \frac{U_{i\max}}{\sqrt{2}U_{n\max}}\right)^{-1}\right] \times U_{i\max}^2\left(1 - \frac{U_{i\max}^2}{2U_{n\max}^2}\right)/P_o. \tag{25}$$

Lf_s can be determined by (11) and (25). In order to reduce the energy storage inductance, f_s should be as large as possible.

The instantaneous value of the energy storage inductance current is (26) as shown at the bottom of the page.

In (26), $U_i{}'$ satisfies

$$U_i{}' = \begin{cases} U_i & [i_L(k-1)T_S < I_L^*] \\ 0 & [i_L(k-1)T_S > I_L^*]. \end{cases} \tag{27}$$

The average value of the energy storage inductance current is

$$I_{Lavg} = \frac{2}{T_n}\int_0^{T_n/2} i_L(t)dt = \frac{2}{T_n}\sum_{k=1}^{N/2}\left[\int_{(k-1)T_S}^{(k-1+D)T_S} i_L(t)dt + \int_{(k-1+D)T_S}^{kT_S} i_L(t)\mathrm{dt}\right] \tag{28}$$

where $N = T_n/T_s$ which is the number of HF switching within one LF output period T_n.

The RMS value of the energy storage inductance current is

$$I_{Lrms} = \sqrt{\frac{2}{T_n}\int_0^{T_n/2} i_L^2(t)\mathrm{dt}} = \sqrt{\frac{2}{T_n}\sum_{k=1}^{N/2}\left[\int_{(k-1)T_S}^{(k-1+D)T_S} i_L^2(t)\mathrm{dt} + \int_{(k-1+D)T_S}^{kT_S} i_L^2(t)\mathrm{dt}\right]}. \tag{29}$$

The peak value of the energy storage inductance current is $i_{L\max}$ in (14).

B. Design for Input Filtering Capacitor

To reduce current ripple of the PV cell, the filtering capacitance C_i is connected in parallel in the input side. The output current of PV cell and filtering capacitor is approximately given by

$$i_i{}'(t) = \frac{U_n I_n}{U_i}[1 - \cos(2\omega t)]. \tag{30}$$

$$i_L(t) = \begin{cases} i_L(k-1)T_S + \dfrac{U_i{}'[t-(k-1)T_S]}{L} & (k-1)T_S < t < (k-1+D)T_S \\ i_L(k-1+D)T_S + \int_{(k-1+D)T_S}^{t} \dfrac{U_i - \left|\sqrt{2}U_n\sin(\omega\tau)\right|}{L}d\tau & (k-1+D)T_S < t < kT_S \end{cases} \tag{26}$$

If the volt–ampere characteristic of PV cell is $i_i = f(u_i)$, since the PV cell in the inverter always operates in near the MPP and the output voltage fluctuation is small, the MPP can be regarded as a static operating point. The output voltage and current of the PV cell can be divided into dc component U_i, I_i and ac component $\tilde{U}_i, \tilde{I}_i$, i.e., $u_i = U_i + \tilde{U}_i, i_i = I_i + \tilde{I}_i,\ dP/du_i|_{u_i=U_i} = 0$, therefore

$$\frac{\mathrm{df}\,(u_i)}{\mathrm{du_i}|_{u_i=U_i}} = -\frac{I_i}{U_i}. \tag{31}$$

From (31), the relationship among the output power P_i, the efficiency η_{PV} and the voltage ripple ratio $\tilde{U}_i/U_i$ of the PV cell can be derived as

$$P_i = U_i I_i \left(1 - \frac{\tilde{U}_i^2}{{U_i}^2}\right) = U_i I_i \eta_{PV}\,. \tag{32}$$

Derived from $i_{Ci} = i_i - i_i'$

$$C_i \frac{\mathrm{d\tilde{U}_i}}{\mathrm{dt}} = f(U_i + \tilde{U}_i) - P_n \frac{1-\cos(2\omega t)}{U_i + \tilde{U}_i} \approx \frac{\mathrm{df(U_i)}}{\mathrm{dU_i}}\tilde{U}_i + \frac{P_n}{U_i}\cos(2\omega t) \tag{33}$$

$$\tilde{U}_i = \frac{P_n \sin(2\omega t + \arctan I_i/(2\omega C_i U_i))}{U_n\sqrt{4\omega^2 {C_i}^2 + (I_i/U_i)^2}}. \tag{34}$$

Set $P_i = P_n$, derived from (32) and (34), the filtering capacitance must be satisfied by

$$C_i \geq \frac{P_n}{2\omega U_i^2}\sqrt{(1-\eta_{\mathrm{PV}})^{-2} - 1}. \tag{35}$$

C. Design for Output CL Filter

The modulation current i_m is mainly composed of fundamental wave whose angular frequency is ω_n and higher harmonic component whose angular frequency is ω_S ($\omega_S = 2\pi/T_S >> \omega$), and L_f, C_f must be satisfied by

$$\frac{1}{\omega_s^2} << L_f C_f << \frac{1}{\omega^2}. \tag{36}$$

CL filter should have enough damping, i.e., the damping factor is given by

$$\xi = \frac{r}{2}\sqrt{\frac{C_f}{L_f}}\,. \tag{37}$$

To make the reactive component produced by u_n as small as possible, it is necessary to further restrict the value of L_f, C_f. Set the fundamental component of modulation current as

$$i_{m1}(t) = \sqrt{2} I_{m1}\sin(\omega t + \theta_m) \tag{38}$$

where θ_m is the angle that i_{m1} leads u_n, so RMS value and phase angle of i_n after filtering are, respectively

$$I_n = \frac{\sqrt{x_C^2 I_{m1}^2 + U_n^2 - 2x_C I_{m1} U_n \sin\theta_m}}{|x_C - x_L|} \tag{39}$$

$$\theta = \tan^{-1}\frac{x_C I_{m1}\sin\theta_m - U_n}{x_C I_{m1}\cos\theta_m} \tag{40}$$

where $x_C = (\omega C_f)^{-1},\ x_L = \omega L_f$. When the same-phase grid-connected $\theta_m = \sin^{-1}(U_n/x_C I_{m1})$, to make θ_m as small as possible, so that

$$\omega C_f U_n << I_{m1}. \tag{41}$$

In parameter selection, (36), (37), and (41) should be considered simultaneously.

VI. Prototype Experiments

Designed example: input dc voltage $U_i = 98 - 122\,\mathrm{V}$, grid voltage $U_n = 220\,\mathrm{V}$ 50 Hz, rated power $P = 1\,\mathrm{kW}$, the switching frequency $f_s = 50\,\mathrm{kHz}$, current sampling frequency selected for 50 kHz, energy storage inductor $L = 1\,\mathrm{mH}$, input filtering capacitor $C_i = 3 \times 1800\,\mu\mathrm{F}$, output filtering capacitor $C_f = 9\,\mu\mathrm{F}$, output filtering inductor $L_f = 0.5\,\mathrm{mH}$, MOSFET IXFK64N50P for S_0–S_4, DSEI60-06A for D and D_1–D_4, LAN25-NP for current sensor, TMS320F28335DSP for control circuit shown in Fig. 3(b).

The experiment waveforms of the designed and developed 1 kW single-phase boost mode PWM grid-connected inverter prototype under the MPP voltage $U_{\mathrm{MPP}} = 110$ VDC and rated full-load with same-phase grid-connected are shown in Fig. 7. The experimental results have shown that: 1) The upper bridge arm switch $S_1(S_2)$ operates in LF and realizes low-voltage turn-on and zero-voltage turn-off, the drain–source voltages $u_{\mathrm{ds1}}, u_{\mathrm{ds2}}$ are both $|u_n|$ with half-output voltage period, as shown in Fig. 7(a) and (b); 2) The lower bridge arm switches S_3, S_4 operate in HF, the drain–source voltage u_{ds3} of S_3 is two-level $(0, u_n)$ PWM wave which is changing according to the sinusoidal envelope of the amplitude u_n or level of the amplitude $U_{m1}(> U_i)$, and the drain–source voltage u_{ds4} of S_4 is two-level $(0, U_i - u_n)$ PWM wave or zero when u_n is positive, $u_{\mathrm{ds3}}, u_{\mathrm{ds4}}$ are the exactly the opposite when u_n is negative, as shown in Fig. 7(c) and (d); 3) S_0 operates in HF, and the drain–source voltage u_{ds0} of S_0 is two-level PWM wave ($|u_n| - U_i$, zero or U_{m2}) which is changing according to the sinusoidal envelope of the amplitude $|u_n| - U_i$ when $|u_n| > U_i$, and $u_{\mathrm{ds0}} = 0$ when $|u_n| < U_i$, as shown in Fig. 7(e); 4) The energy storage inductor current i_L is, respectively, gradually increasing and deviates from ${I_L}^*$ around zero point and pulsing around ${I_L}^*$ with low double frequency component in other intervals, as shown in Fig. 7(f); 5) i_{L} is modulated into unipolarity three-state current wave i_m by inverting bridge, as shown in Fig. 7(g) and (h); 6) The grid-connected current's THD is 2.0%, its RMS value is 4.55 A, the grid side power factor is 0.998, as shown in Fig. 7(i); 7) The start-up and stabilization time of the output current of the PV cell and the grid-connected current is about 0.1 s, as shown in Fig. 7(j); and 8) The experimental waveforms and the expended waveforms for light intensity fast change (100–500 –1000 W/m^2) shown in Fig. 7(k) and (l) have shown that the system has fast dynamics response, and the dynamics response time is about 0.1 s.

The conversion efficiency and grid-connected current's THD of the proposed inverter under three kinds of different MPP voltage are shown in Fig. 8.

Experimental results have shown that: 1) The conversion efficiency of the inverter under three kinds of MPP voltage 98,

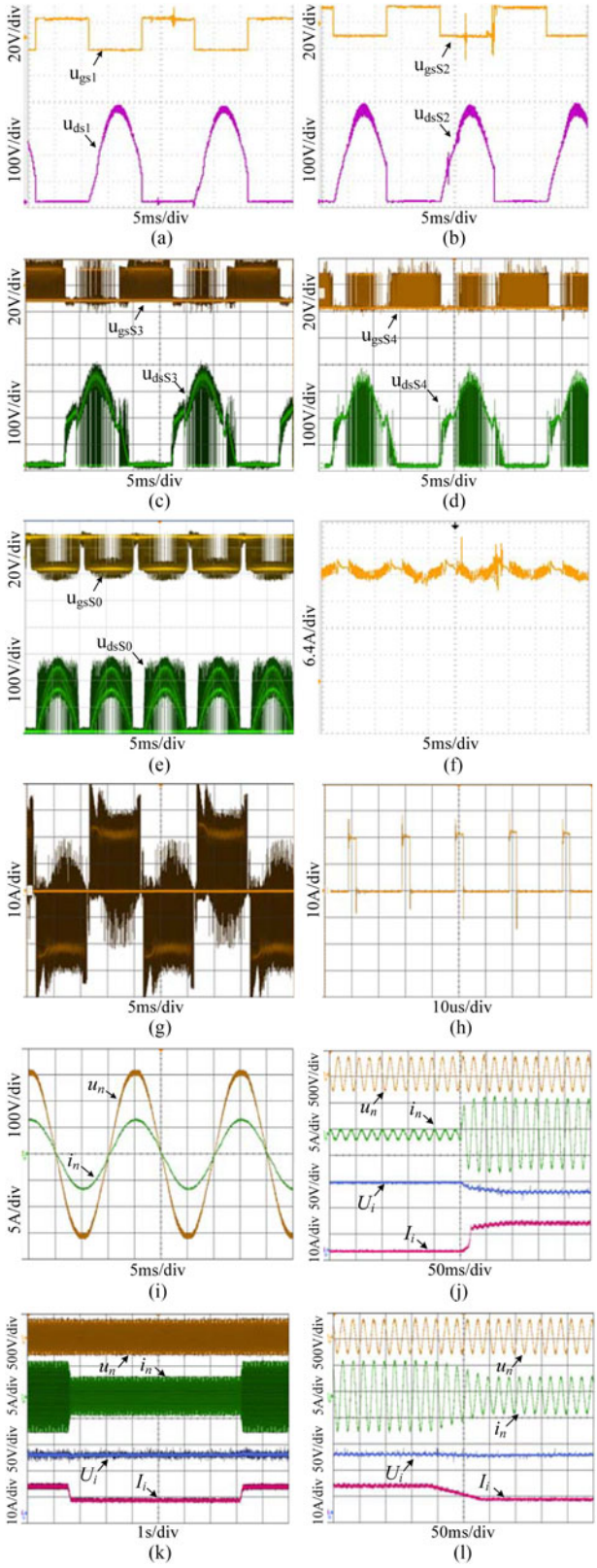

Fig. 7. Experimental waveforms of the proposed inverter under the MPP voltage $U_{\mathrm{MPP}} = 110$ VDC and rated full-load. (a) u_{gs1} and u_{ds1} of S_1, (b) u_{gs2} and u_{ds2} of S_2, (c) u_{gs3} and u_{ds3} of S_3, (d) u_{gs4} and u_{ds4} of S_4, and (e) u_{gs0} and u_{ds0} of S_0. (f) Energy storage inductor current i_L. (g) LF modulating current i_m. (h) HF expanded modulating current i_m. (i) Grid voltage u_n and grid-connected current i_n. (j) Waveforms at start up. (k) Waveforms for light intensity. (l) Expanded waveforms for light fast change intensity fast decreasing.

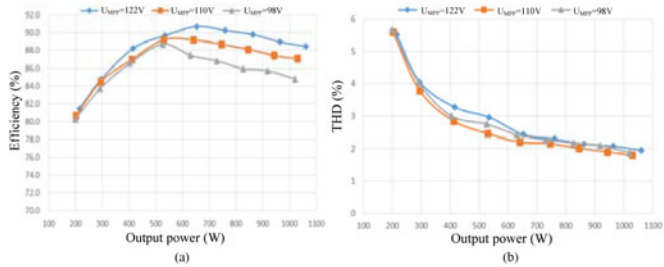

Fig. 8. Conversion efficiency and grid-connected current's THD of the proposed inverter under three kinds of different MPP voltage. (a) Conversion efficiency. (b) Grid-connected current's THD.

110, 122 V and full load are 84.76%, 87.10%, and 88.46%, respectively, and the maximum efficiency is achieved at about 600 W output power; 2) THD of grid-connected current of the inverter is monotonously decreasing with the increase of load, and all THD under three kinds of MPP voltage and full load are less than 2.0%. The loss of the inverter mainly includes conduction loss of five pair of power switches and blocking diode, the iron loss and copper loss of the energy storage inductor. The inherent loss of the inverter dominates under light load, and the conduction loss of five pair of power switches and blocking diode, the copper loss of the energy storage inductor dominates under heavy load. For the same output power, $I_L{}^*$ decreases with U_i increasing; the loss of the inverter decreases, its efficiency is increased. Especially when $U_{\mathrm{MPP}} = 122\,\mathrm{V}$, the maximum efficiency of the inverter is 90.71%. With the development and application of the bidirectional blocking power device such as the reverse-blocking IGBT, the proposed inverter will be not necessary to connect in series with the reverse blocking diode, and the conversion efficiency will be greatly improved. The lighter the load, the larger the grid-connected current's THD, because there are larger measurement error of AD and current transducer with larger scale under the light load.

The advance of the inverter's performance is the result of both novel topology and control strategies. From the topology point of view, a combined circuit topology is adopted in [11], whose energy storage inductance is small but the output filter is large, the conversion efficiency is only 78%, and THD of output voltage is as high as 3.87%. The traditional circuit topology is adopted in [13] and [14], and the energy storage inductance is as high as 10–21 mH. A parallel resonator is added based on the traditional circuit topology in [15], which reduces value of the energy storage inductor to 5 mH, but two resonant inductance and resonant capacitance are added. A bypass switch is connected in parallel on both ends of the energy storage inductor, which significantly reduces value of the energy storage inductance to 1 mH and ensures high conversion efficiency. From the control strategy point of view, Li *et al.* [13] adopt active nonlinear control strategy that reduces grid-connected current's THD to 4.42%, but the output filter is still large. A control strategy based on the inverter's output current involving feedforward and feedback terms is adopted in [14], which improves quality of the output voltage, but the conversion efficiency and THD of the output voltage are not provided; Alajmi *et al.* [15] use the output voltage and current feedback control strategy with proportional resonance, which reduce the output waveform's THD to 2%,

but the output filter is still large, and only experimental waveforms under light load is provided; the proposed control strategy makes output waveform with low THD and small output filter. The single-phase boost mode inverter's topology which does not meet the basic principle of boost converter is very different from the three-phase boost mode inverter's topology in [6] which meets the basic principle of boost converter; the proposed nonlinear control strategy real time adjusts the inverter's regenerating energy duty ratio 1–*D* which decreases with the decline of the grid-connected voltage $u_{\rm n}$ by sampling and feeding back the inverting bridge modulation current, and the average value of the modulation current in each switching cycle tracks the reference sinusoidal signal to get high quality grid-connected current; whereas the one-cycle control strategy in [6] regulates the inverter's energy storage duty ratio *D* which decreases with the decline of the grid-connected line voltage by sampling and feeding back the energy storage inductor current, and the average value of the difference between constant related to output power and the energy storage inductor current in each switching cycle tracks the reference line voltage to get grid-connected current with THD value of 5%. Therefore, the proposed nonlinear control strategy which can solve the inherent defect of the single-phase boost mode inverter has some difference from the one-cycle control strategy in [6]. The comparison results have shown that the proposed inverter obtains excellent comprehensive performance indexes such as small energy storage inductor and output filter, small THD of grid-connected current waveform, high conversion efficiency, low cost, etc.

VII. Conclusion

1) A nonlinear PWM control strategy based on inverting bridge modulation current is proposed. The size of 1–*D* is timely adjusted by detecting and feeding back modulation current i_m, and the quality of output waveform is improved.
2) A circuit topology of the single-phase boost mode grid-connected inverter with additional bypass switch of the energy storage inductor and two types of switching pattern with limitation current of the energy storage inductor is proposed. The active control of the energy storage inductor current is realized by the freewheeling state of energy storage inductor replacing the magnetizing state. The problems such as excess energy of the energy storage inductor and too large step-up ratio of the inverter can be effectively solved and the conversion efficiency is also improved.
3) There are six kinds of equivalent circuits and eight operating intervals in one LF output period; there are four kinds of operating situations and eight operating intervals in one HF switching period, and the relationship between step-up ratio and duty ratio of the equivalent switch is derived.
4) Design criteria of the key parameters such as the energy storage inductor, limitation current of energy storage inductor, input and output filter are derived.
5) The experimental results of the designed and developed 1 kW 110 VDC/220 V 50 Hz AC inverter prototype show that the energy storage inductance is significantly reduced, conversion efficiency is increased, and the quality of output waveform is improved.

References

[1] M. K. Nguyen, T. V. Le, S. J. Park, and Y. C. Lim, "A class of quasi-switched boost inverters," *IEEE Trans. Ind. Electron.*, vol. 62, no. 3, pp. 1526–1536, Jul. 2015.

[2] S. S. Nag and S. Mishra, "Current-fed switched inverter," *IEEE Trans. Ind. Electron.*, vol. 61, no. 9, pp. 4680–4690, Nov. 2014.

[3] B. Singh, C. Jain, and S. Goel, "ILST control algorithm of single-stage dual purpose grid connected solar PV system," *IEEE Trans. Power Electron.*, vol. 29, no. 10, pp. 5347–5357, Dec. 2014.

[4] Y. Tang, X. Dong, and Y. He, "Active buck-boost inverter," *IEEE Trans. Ind. Electron.*, vol. 61, no. 9, pp. 4691–4697, Dec. 2014.

[5] J. R. Espinoza and G. Joos, "A current-source-inverter-fed induction motor drive system with reduced losses," *IEEE Trans. Ind. Appl.*, vol. 34, no. 4, pp. 796–805, Aug. 1998.

[6] Y. Chen and K. Smedley, "Three-phase boost-type grid-connected inverter," *IEEE Trans. Power Electron.*, vol. 23, no. 5, pp. 2301–2309, Sep. 2008.

[7] Q. Lei, D. Cao, and F. Z. Peng, "Novel loss and harmonic minimized vector modulation for a current-fed quasi-z-source inverter in HEV motor drive application," *IEEE Trans. Power Electron.*, vol. 29, no. 3, pp. 1344–1357, May 2014.

[8] Y. Tang, S. J. Xie, C. H. Zhang, "Single-phase Z-Source inverter," *IEEE Trans. Power Electron.*, vol. 26, no. 12, pp. 3869–3873, Feb. 2011.

[9] R.O. Caceres and I. Barbi, "A boost DC-AC converter: Analysis, design, and experimentation," *IEEE Trans. Power Electron.*, vol. 14, no. 1, pp. 134–141, Jan. 1999.

[10] Y. Fang and X. Ma, "A novel PV microinverter with coupled inductors and double-boost topology," *IEEE Trans. Power Electron.*, vol. 25, no. 12, pp. 3139–3147, Oct. 2010.

[11] L. S. Garcia, L. C. de Freitas, G. M. Buiatti, E. A. A. Coelho, V. J. Farias, and L. C. G. Freitas, "Modeling and control of a single-stage current source inverter with amplified sinusoidal output voltage," in *Proc. 27th IEEE Appl. Power Electron. Conf. Expo.*, 2012, pp. 2024–2031.

[12] D. Chen, J. Zhang, and Y. Chen, "Development and present states of the power electronic conversion technologies with high frequency link," *CPES J. Power Electron.*, vol. 48, no. 6, pp. 1–11, Jun. 2014 (in Chinese).

[13] R. T. H. Li, H. S. H Chung, and T. K. M. Chan, "An active modulation technique for single-phase grid-connected CSI," *IEEE Trans. Power Electron.*, vol. 22, no. 4, pp. 1373–1382, Jul. 2007.

[14] H. Komurcugil, "A new control strategy for single-phase PWM boost-type inverters," in *Proc. 37th Annu. Conf. IEEE Ind. Electron. Soc.*, 2011, pp. 1063–1068.

[15] B. N. Alajmi, K. H. Ahmed, G. P. Adam, and B. W. Williams, "Single-phase single-stage transformer less grid-connected PV system," *IEEE Trans. Power Electron.*, vol. 28, no. 6, pp. 2264–2676, Nov. 2013.

Daolian Chen (SM'08) was born in Fujian, China, in 1964. He received the B.S., M.S., and Ph.D. degrees, and Postdoctoral Certification from the Department of Electrical Engineering, Nanjing University of Aeronautics and Astronautics (NUAA), Nanjing, China, in 1986, 1989, 1998, and 2001, respectively.

He was a Teaching Assistant, Lecturer, Associated Professor, Professor with the Department of Electrical Engineering, NUAA, in 1989, 1991, 1996, and 2002, respectively. He has been a Professor with the College of Electrical Engineering, Fuzhou University, Fuzhou, China, since 2005. He has been a "National Class Expert of the Hundred, Thousand, and Ten Thousand Talent Project," "Delta Scholar," and "National outstanding professional and technical personnel," China, since 2009, 2014, and 2014. He has been the Director of the Fujian Key Laboratory of New Energy Generation and Power Conversion, since 2015. He has published three works and more than 100 technical papers. He is the holder of 20 invention patents. His research interests include power electronics conversion, new energy source generating, and aviation electrical power supply systems.

Dr. Chen was awarded one national and three province class reward productions of science and technology.

Yanhui Qiu was born in Fujian, China, in 1988. He received the B.S. degree from the College of Electrical Engineering, Fuzhou University, Fuzhou, China, in 2011, where he is currently working toward the Ph.D. degree in the Fujian Key Laboratory of New Energy Generation and Power Conversion.

He has published several technical papers. His research interests include new energy source generating.

Yiwen Chen was born in Fujian, China, in 1977. She received the B.S., M.S., and Ph.D. degrees in electrical engineering from Fuzhou University, Fuzhou, China, in 2000, 2004, and 2015, respectively.

She is currently a Lecturer in the Fujian Key Laboratory of New Energy Generation and Power Conversion, Fuzhou University. She has published almost ten technical papers. She is the holder of about ten invention patents. Her research interests include new energy source generating.

Yongji He was born in Fujian, China, in 1990. He received the B.S. and M.S. degrees in electrical engineering from Fuzhou University, Fuzhou, China, in 2012 and 2015, respectively.

He is currently an Engineer in JoulWatt Technology, Inc., Limited, Hangzhou, Zhejiang, China. He has published several technical papers. His research interests include high frequency power conversion.